The Spreading of Lower Circumpolar Deep Water in the Atlantic Ocean

REINER ONKEN

Institut für Meereskunde, Düsternbrooker, Kiel, Germany

(Manuscript received 1 August 1994, in final form 3 March 1995)

ABSTRACT

A Stommel–Arons model of the circulation of Lower Circumpolar Deep Water (LCDW) in the Atlantic Ocean is presented and compared with observations. The LCDW is defined as a layer of uniform thickness over a flat bottom; the lateral boundaries are given by the 4000-m isobath. The Drake Passage and the throughflow between Africa and Antarctica are closed. The model is forced by a concentrated source in the Weddell Sea representing the net Atlantic gain of LCDW due to production in the Weddell Sea and inflow through Drake Passage. This net gain is termed the LCDW formation rate. It is compensated by upwelling over the rest of the Atlantic.

Best agreement with observed net transport rates in the western Atlantic was found using a LCDW formation rate of about 8 Sv (Sv $\equiv 10^6$ m^3 s^{-1}). In reality, however, a higher rate is required in order to establish the outflow to the Indian Ocean. The interior transport, the transport through topographic gaps, and the transport rates of western boundary currents on the eastern flanks of topographic barriers are calculated and compared with observations where available.

In additional runs it was found that raising the production rate to a value of 13 Sv and enabling simultaneously an LCDW outflow of 5 Sv into the Indian Ocean can explain observed very high transport rates in the South Sandwich Trench. Consequences of different patterns of nonuniform upwelling are discussed.

1. Introduction

The Lower Circumpolar Deep Water (LCDW) is the dominant water mass found next to the sea floor of the World Ocean. It originates from sinking of surface water at distinct locations around Antarctica and subsequent mixing with other water masses. This newly formed water is dragged around Antarctica by the Circumpolar Current and finally invades the abyss of the Atlantic, Indian, and Pacific Oceans, where it is further diluted by mixing with the overlying water masses. The southern origin, however, can still be identified by its low salinity, low oxygen, and high silica content (Emery and Meincke 1986; Warren 1981; Mantyla and Reid 1983).

Two major sources contribute to the LCDW found in the Atlantic Ocean—very dense and cold Weddell Sea Deep Water (WSDW) (potential temperatures below about 0°C, $\sigma_4 > 46.07$ kg m^{-3}) and less dense, warmer LCDW (potential temperatures between about 0° and 2°C, 45.85 kg m^{-3} $< \sigma_4 <$ 46.07 kg m^{-3}) coming from the west through Drake Passage (Reid et al. 1977). At present it is still unknown to what extent Drake Passage LCDW enters the abyss of the Atlantic Ocean, but there exist some crude estimates of the WSDW fraction contributing to the Atlantic LCDW. According to Foster and Carmack (1976), WSDW is formed by mixing of Weddell Sea Bottom Water (WSBW) with the overlying Warm Deep Water (WDW) in the ratio of about 1:1. The WSBW formation rate ranges from 2–5 Sv (Sv $\equiv 10^6$ m^3 s^{-1}) (Carmack and Foster 1975) to 6–9 Sv (Gill 1973); hence, WSBW should form at a rate between 4 and 18 Sv. Assuming the total volume of WSBW in the Weddell Sea to be constant, an amount equal to the newly formed WSDW has to exit. According to Gordon (1966), Carmack (1977), Reid (1989), and Whitworth et al. (1991), this happens either to the north via the South Sandwich Trench into the Argentine Basin or to the east into the Cape–Agulhas Basin and Indian Ocean. For the first pathway, the geostrophic calculations of Georgi (1981) yielded a net volume flux of ~15 Sv at the southern entrance of the Trench and 5 Sv at the northern end; the amount of WSDW transferred into the Cape–Agulhas Basin and the Indian Ocean, however, has never been quantified from measurements. The existence of the outflow is confirmed by Mantyla and Reid's (1983) maps of scalar near-bottom properties, and the inverse calculations of Rintoul (1991) suggest eastward volume transports into the Indian Ocean from 5 to 10 Sv for potential temperatures below 0.4°C based on reasonable assumptions on the structure of the global thermohaline circulation pattern.

Corresponding author address: Dr. Reiner Onken, Institut für Meereskunde, an der Universitat Kiel, Düsternbrooker Weg 20, D-24105 Kiel, Germany.

In the Atlantic, LCDW is found in all basins. From the Argentine Basin it flows north and invades the Brazil Basin via the Vema and Hunter Channels and the Lower Santos Plateau (Hogg et al. 1982; Speer et al. 1992; Speer and Zenk 1993). At the northern end of the Brazil Basin, the flow splits into an eastward branch through the Romanche Fracture Zone and a northwestward one, which spills over the broad equatorial sill into the Guiana Basin (McCartney and Curry 1993) and finally into the North American Basin (Amos et al. 1971; Tucholke et al. 1973), where it can be identified up to 40°N (Weatherly and Kelley 1982, 1985). The eastern North Atlantic, that is, the Cape Verde, Canary, and Iberian Basins, are supplied via the Vema Fracture Zone at ≈11°N (Vangriesheim 1980; Eittreim et al. 1983; McCartney et al. 1991). Here LCDW influence has been traced northward up to ~32°N (Saunders 1987). The Sierra Leone and Angola Basins get their LCDW contribution through the Romanche Fracture Zone from the Brazil Basin; however, the abyss of the southwesternmost corner of Angola Basin is also partly influenced by LCDW, which originates from the Cape–Agulhas Basin and spills over deep sills in the Walvis Ridge named the "Walvis Passage" after Connary and Ewing (1974).

There have been various attempts to quantify the LCDW flow in the Atlantic basins and the exchange rates between them by measurements, a summary of which is given in Table 1. However, except for the general impression that in the western basin the transport values decrease with increasing latitude, the measurements yield a rather inconsistent transport pattern. This is probably due to the following reasons.

- The majority of the transports have been calculated by applying the dynamical method to density measurements, the results of which depend critically on the choice of the level of no motion (see Table 1: "reference level").
- Different authors have used different definitions for the LCDW (see Table 1: "LCDW definition").
- The measured transports are related to different quantities. Many of them refer to basinwide integrated net transports, whereas others are confined to the western boundary, and others to flows through topographic gaps (see Table 1: "remarks").

In the present paper, an attempt is made to develop a consistent LCDW circulation scheme for the Atlantic Ocean by using a linear Stommel–Arons model, which relates the flow in the interior of the LCDW containing layer to the vertical motion imposed on the upper boundary. The vertical motion pattern is driven by a concentrated source (downwelling) in the Weddell Sea representing the net gain of Atlantic LCDW due to production in the Weddell Sea and inflow through Drake Passage, that is, the sum of total LCDW production in the Weddell Sea and LCDW inflow through Drake Passage minus the LCDW outflow to the Indian Ocean. The input by the source is compensated by sluggish upwelling occuring over the rest of the Atlantic. Because the source strength and the upwelling pattern are fairly unknown, the modeled volume transports are calibrated against observed transports in the western Atlantic basin. In this way a lower bound can be imposed on the net inflow of LCDW into the Atlantic Ocean.

It was originally intended to develop a more complex model of the LCDW circulation in the Atlantic Ocean, including meridional and zonal bottom slopes and the south–north tilt of the interface between LCDW and North Atlantic Deep Water (cf. Wright 1970, Fig. 1). However, an inspection of the results of a preliminary run using a flat bottom and a horizontal interface revealed so many interesting features that it seemed worthwhile to publish it in a separate study first.

2. The model

a. Equations

In the model, LCDW is represented by a layer of constant thickness H bounded by a flat bottom at $z = 0$. Using spherical coordinates, the linearized vorticity equation for the vertically integrated meridional velocity $V = \int_0^H v\,dz$ reads

$$V(\lambda, \varphi) = -wR \tan\varphi, \tag{1}$$

assuming hydrostatic balance and neglecting friction and tidal forces. In a meridionally bounded basin the vertically integrated zonal velocity $U = \int_0^H u\,dz$ at any constant latitude $\varphi = \varphi_0$ is obtained by integrating the continuity equation from the eastern boundary, $\lambda = \lambda_E$, assuming zero normal velocity there:

$$U(\lambda, \varphi_0) = -\int_{\lambda_E}^{\lambda} \frac{\partial}{\partial\varphi}(V\cos\varphi_0)\,d\lambda' - R\cos\varphi_0 \int_{\lambda_E}^{\lambda} w(\lambda', \varphi_0)\,d\lambda'. \tag{2}$$

In (1) and (2) w represents the vertical velocity imposed on top of the layer, and the bottom vertical velocity has been set to zero. The other symbols used have the conventional meanings:

R	earth radius = 6371 km,
u	zonal velocity,
v	meridional velocity,
z	vertical coordinate, $z = 0$ at the bottom, increasing upward,
φ	latitude, $\varphi = 0$ at the equator, increasing northward,
λ, λ'	longitude, $\lambda, \lambda' = 0$ at the Greenwich meridian, increasing eastward.

b. Basin geometry, boundary conditions, and western boundary currents

In the model, a C-grid with $\Delta\lambda \times \Delta\varphi = 1° \times 1°$ is used. The model domain is represented by those areas

TABLE 1. Observed transports of Lower Circumpolar Deep Water in the Atlantic Ocean (eastward, northward > 0. Temperature values are potential temperatures).

Author	Method	Reference level	LCPW definition	Latitude/longitude (degrees)	Transport (Sv)	Remarks
			Western basin			
Weatherly and Kelley (1982)	C	1.82°C	<1.82°C	40N	−0.5	WB
Tucholke et al. (1973)	D, C	4700 m	<1.84°C	23N	0.5	net (1)
Wright (1970)	D	2°C	<2°C	16N	1.4	net
Wright (1970)	D	2°C	<2°C	~10N	2.7	net (2)
Wright (1970)	D	2°C	<2°C	8N	2.7	net
McCartney (1994)	D	1.9°C	<1.9°C	4N	4.0	net
Whitehead and Worth. (1982)	C	1.9°C	<1.9°C	4N	0.8	WB
Whitehead and Worth. (1982)	D	1.9°C	<1.9°C	4N	2.0	net
Sverdrup et al. (1942)	?	?	?	0N	1.0	net
McCartney and Curry (1993)	D	4000 dbar	<1.93°C	0N	4.3	net
Wright (1970)	D	2°C	<2°C	8S	2.8	net
McCartney and Curry (1993)	D	4000 dbar	<1.9°C	11S	5.5	net
Speer and Zenk (1993)	D	2°C	<2°C	11S	3.0	net
Wright (1970)	D	2°C	<2°C	16S	2.3	net
Speer and Zenk (1993)	D	2°C	<2°C	19S	4.5	net
McCartney and Curry (1993)	D	1.9°C	<1.9°C	23S	6.7	net
Wright (1970)	D	2°C	<2°C	24S	6.4	net
Speer and Zenk (1993)	D	2°C	<2°C	24S	5.0	net
Sverdrup et al. (1942)	D	?	?	30S	3.0	net
Hogg et al. (1982)	D, C	1.8°C	<1.8°C	30S	4.1	Vema
Speer and Zenk (1993)	D	2°C	<2°C	30S	2.0	Santos
Speer and Zenk (1993)	D	2°C	<2°C	31S	6.7	net
Wright (1970)	D	2°C	<2°C	32S	5.1	net
Speer et al. (1992)	D	2°C	<2°C	34S	0.7	Hunter
Georgi (1981)	D	1°C	<1°C	40S	10.0	WB
Georgi (1981)	D	0°C	<0°C	40S	1.8	WB
Georgi (1981)	D	0°C	<0°C	46S	1.0	WB
Whitworth et al. (1991)	C	0.2°C	<0.2°C	50S	8.2	WB
Georgi (1981)	D	0°C	<0°C	51S	1.3	WB
Georgi (1981)	D	0°C	<0°C	54S	5.0	WB
			Weddell-Enderby Basin			
Georgi (1981)	D	0°C	<0°C	56S	12.0	WB
Georgi (1981)	D	0°C	<0°C	56S	5.0	net
Georgi (1981)	D	0°C	<0°C	59S	15.0	net
Georgi (1981)	D	0°C	<0°C	59S	18.0	WB
			Eastern basin			
Saunders (1987)	C	2.05°C	<2.05°C	37N	0.21	Discovery
Saunders (1987)	D	3500 dbar	<2.05°C	37N	0.35	Discovery
Saunders (1987)	C	3500 dbar	<2.05°C	36N	0.7	net
McCartney et al. (1991)	D	2–2.5°C	<2°C	36N	0.46	net
McCartney et al. (1991)	D	2–2.5°C	<2°C	36N	0.83	east
McCartney et al. (1991)	D	2–2.5°C	<2°C	36N	−0.37	WB
McCartney et al. (1991)	D	2–2.5°C	<2°C	36N	0.58	net
McCartney et al. (1991)	D	2–2.5°C	<2°C	35W	1.55	WB, mean
McCartney et al. (1991)	D	2–2.5°C	<2°C	24N	1.1	WB
McCartney et al. (1991)	D	2–2.5°C	<2°C	15N	1.9	WB
McCartney et al. (1991)	D	2–2.5°C	<2°C	9N	0	Kane Gap
McCartney et al. (1991)	D	2–2.5°C	<2°C	29W	1.0	Gambia
Warren and Speer (1991)	D	4000 dbar	<4000 dbar	11S	−0.75	WB
Warren and Speer (1991)	D	4000 dbar	<4000 dbar	11S	−1.16	net
Warren and Speer (1991)	D	4000 dbar	<4000 dbar	24S	2.45	WB
Warren and Speer (1991)	D	4000 dbar	<4000 dbar	24S	−0.7	net
			Vema Fracture Zone			
Vangriesheim (1980)	C	1.5°C	<1.5°C	11N	0.46	
McCartney et al. (1991)	D	2.17°–2.43°C	<2°C	11N	2.2	mean

C: current meters; D: dynamical method; Discovery: Discovery Gap; east: in eastern part of the basin; Gambia: transport along southern boundary of Gambia Abyssal Plane; Hunter: transport through Hunter Channel; Kane Gap: Kane Gap throughflow; net: net meridional basinwide transport; Santos: transport over Lower Santos Plateau; Vema: transport through Vema Channel; WB: western boundary current transport; (1): net northward transport estimated from their Table 2 and Fig. 6; (2): meridional section at 50°W.

of the Atlantic Ocean, where the water depth is greater than 4000 m (Fig. 1). The Atlantic–Indian throughflow is closed. Because the interior flow is completely determined by (1) and (2) if $w(\varphi, \lambda)$ is known and no normal flow is allowed at the lateral boundaries, the vertical volume flux across the top interface and integrated over the model domain must vanish.

Due to (2) continuity is satisfied everywhere except at western boundaries of the domain, where a volume flux deficit may arise due to the no-normal-flow constraint. Therefore, an infinitesimally wide western boundary layer is introduced, where a western boundary current (WBC) compensates for the deficit. The WBC is evaluated by integrating up the volume flux deficits along the western sidewalls of grid cells neighbored by land cells in the west. This implies also pieces of zonal boundary currents along zonal segments of grid cells separating land and sea.

Because of the complicated topographic shape of the model domain, there are seven WBCs numbered from 1 to 7 (Fig. 2). These are the northern and the southern Cape–Agulhas Basin WBCs (Nos. 1, 2), the Angola Basin (No. 3), the northeast Atlantic (No. 4), the eastern tropical Atlantic (No. 5), the Hunter Channel (No. 6), and the western Atlantic WBC (No. 7). For continuity reasons, the integration of WBCs Nos. 1 and 4 starts at the most northern extension of the respective basin, the integration of No. 3 starts at the most southern extension of the Angola Basin, and No. 7 is integrated from south to north. A special problem arises for WBCs Nos. 6 and 5 attached to the east coast of the two "islands," that is, the Rio Grande Rise and that part of the Mid-Atlantic Ridge between the Vema Fracture Zone and the Romanche Fracture Zone. Here, the starting point of the integration can be chosen arbitrarily at the northern or the southern tip of the islands without violating continuity, and there are two possible solutions for the direction of the boundary currents (cf. Warren and Speer 1991). In the present paper, the starting point for the integration of WBC No. 6 is in the south and that for WBC No. 5 in the north. This choice leads to WBC flow directions in agreement with observations (Speer et al. 1992; Metcalf et al. 1964; Hee-

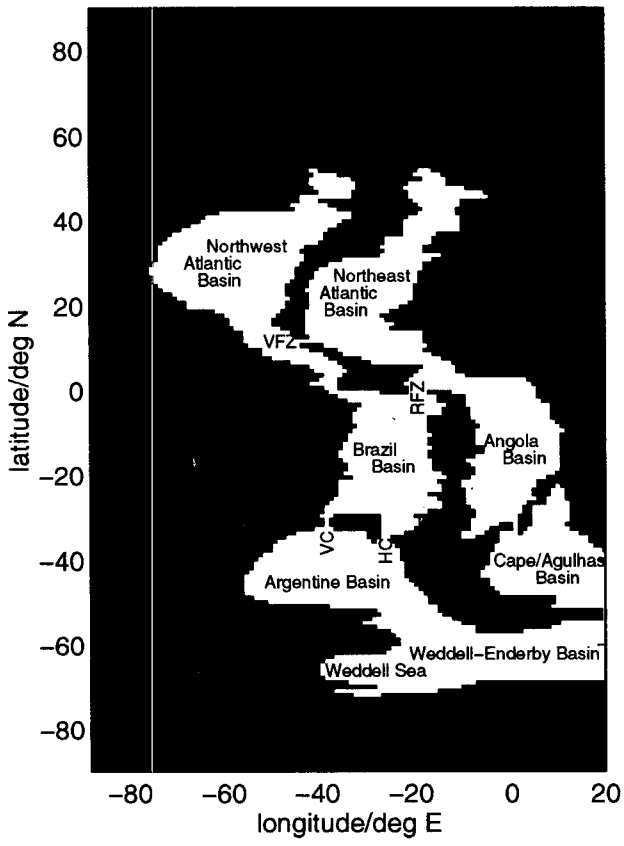

FIG. 1. The model domain (white) is represented by those parts of the Atlantic that are deeper than 4000 m. The throughflow between South Africa and Antarctica is closed (VC = Vema Channel, HC = Hunter Channel, RFZ = Romanche Fracture Zone, VFZ = Vema Fracture Zone).

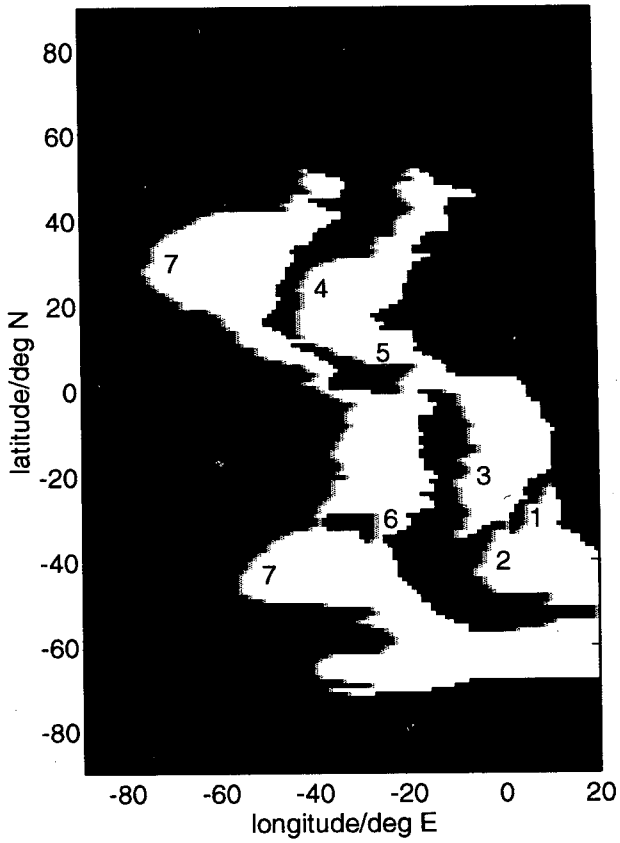

FIG. 2. There are seven western boundary currents (WBC) in the model: the northern Cape–Agulhas Basin (1), southern Cape–Agulhas Basin (2), Angola Basin (3), Northeast Atlantic (4), eastern tropical Atlantic (5), Hunter Channel (6), and western Atlantic WBC (7). Light gray shading indicates the infinitesimally wide western boundary layer.

zen et al. 1964). In order to prohibit a sign change of the Cape–Agulhas Basin WBCs Nos. 1 and 2 at the Walvis Passage, the integration of No. 2 is starting in the north.

The integration of each WBC is finished at the most southern (WBCs Nos. 1, 2, 4, 5, 7) or the most northern extension (Nos. 3 and 6) of the western boundary layer. The final value represents the interior volume flux deficit (positive or negative) of the respective basin and is then added to the flux deficit of that western boundary layer encountered next in the west at the same latitude. Because that means that WBC No. 1 is feeding No. 2, No. 3 is feeding No. 5, and WBCs Nos. 2, 4, 5, and 6 are feeding the western Atlantic WBC No. 7, the WBC transports have to be calculated in the sequence 1, 2, 3, 4, 5, 6, and 7. This is a different interpretation of the continuity equation (2), where the source on the right-hand side driven by vertical transports is replaced by a source due to the volume flux surplus–deficit of the WBC at the respective grid point.

3. Model calibration

The LCDW gain of the Atlantic from the inflow through Drake Passage and production in the Weddell Sea is represented by a concentrated source in the Weddell Sea and expressed in terms of vertical transport concentrated at a single grid point. The strength of this source is called the "LCDW formation rate." Applying the simple assumption of compensating uniform upwelling over the rest of the model domain, it is an easy task to calculate the LCDW transport in the interior of the basins and the corresponding WBC transports. The formation rate of Atlantic LCDW, however, is not well known. Therefore, the modeled LCDW transports will be calibrated against the observed net meridional flow in the western Atlantic (cf. Table 1), that is, the zonally integrated flow in the Argentine, Brazil, and Northwest Atlantic Basins. The western Atlantic is chosen because the majority of observations were located there. The observed net meridional transports are displayed in Fig. 3. A linear regression yields a correlation coefficient of 0.73, which means that a linear decrease of meridional LCDW transport with increasing latitude is an acceptable approximation.

A series of model runs driven by different LCDW formation rates were performed, and the net meridional flow in the western basin was compared with the linear regression mentioned before (Fig. 4). In order to visualize the sensitivity of the meridional transport to the choice of the formation rates, the transport curves assuming 6, 8, or 10 Sv, respectively, are shown, where the sinking occurs in a single grid cell centered at 67°S, 47°W in the western Weddell Sea. It can be seen clearly that the first yields too low transports over nearly the entire latitude range, and the transports of the latter are too high. The best agreement was found for a model run assuming a formation rate of ~8 Sv.

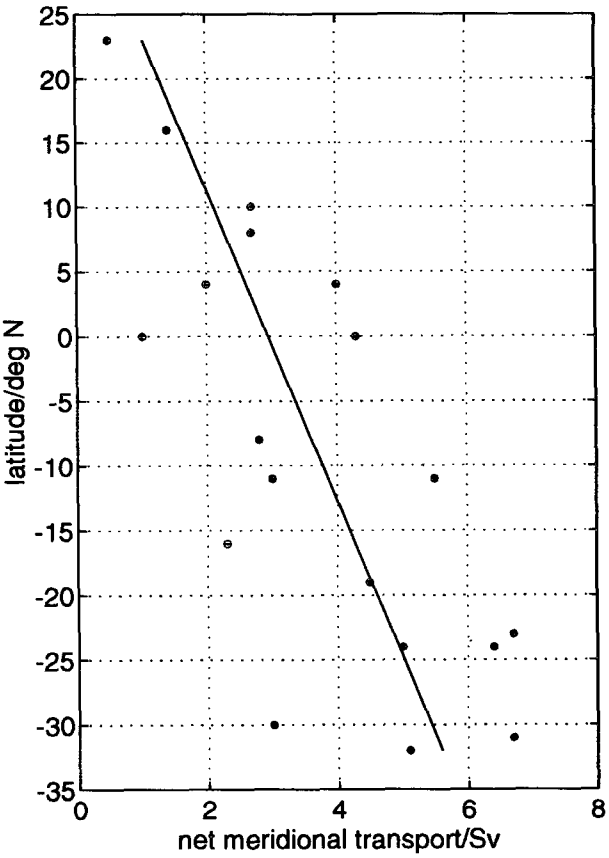

FIG. 3. Observed net meridional transport (dots) of LCDW in the western Basin of the Atlantic Ocean (cf. Table 1). The correlation coefficient of the linear regression is 0.73.

4. Model results and comparison with observations

In the preceeding section it was found that the assumption of a LCDW formation rate of $S_0 \approx 8$ Sv matches best the net meridional transport in the western basin. In the following, the results of that model run named STDRD will be investigated in more detail. First, the western boundary currents will be shown; second the interior transport outside the western boundary layer is given; and third the net transport in individual basins is presented.

It should be mentioned that S_0 is only that fraction of the formation rate that is necessary to establish the LCDW circulation pattern in the Atlantic. In reality, however, the formation rate must be higher because an unknown amount of LCDW is needed to supply the LCDW layer of the Indian and (perhaps) the Pacific Oceans. Therefore, in the discussion section effects are discussed that are due to an outflow of LCDW into the Indian Ocean.

a. Western boundary currents

The latitudinal dependence of WBC transports is displayed in Fig. 5 and in a summary sketch in Fig. 6. The

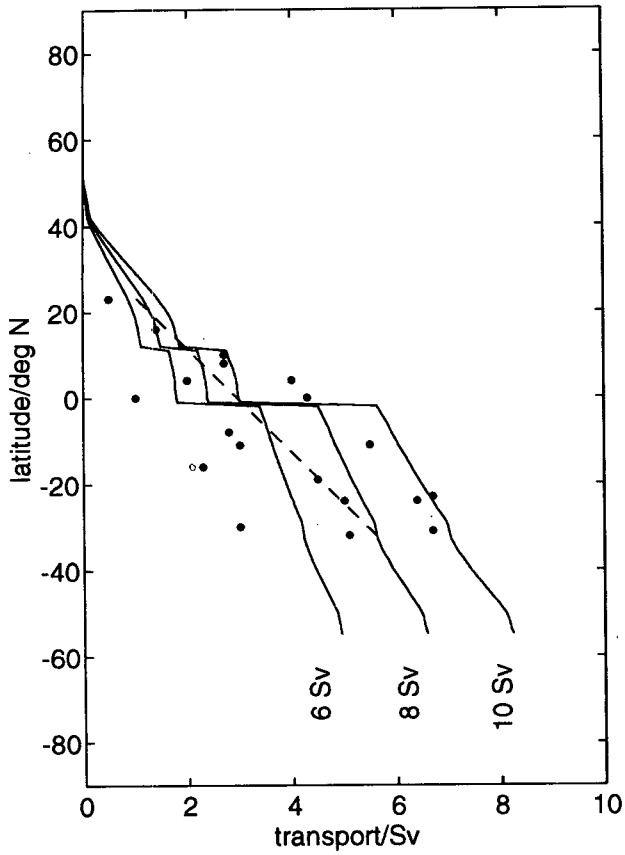

FIG. 4. Modeled net meridional transport (solid lines) in the western Atlantic basin assuming 6, 8, or 10 Sv LCDW production rate. The dashed line represents the linear fit displayed in Fig. 3; observed transports are marked by dots (cf. Fig. 3).

largest transport rates of nearly 14.7 Sv northward can be found in the western Atlantic WBC No. 7 at 66°S. Farther north, the transport decreases nearly linearly at a rate of about 0.16 Sv per degree and drops to zero at 22°N. North of that latitude, the WBC reverses direction and exhibits maximum southward transport of 2.1 Sv at 40°N. For comparison, there are only a few observed transports available. At 59°S and 56°S, Georgi (1981) calculated geostrophic WBC transports of 18.0 and 12.0 Sv (cf. Table 1), which are 6 or 4 Sv, respectively, higher than the model values. These numbers, however, refer to the transport of water colder than 0°C, which stems from the Weddell Sea only. Between 54° and 40°S Georgi's (1981) geostrophic transport calculations yield results between 1 and 10 Sv, the magnitude of which seems to be very sensitive to the choice of the reference level. At 40°S, for example, the transport using the 1°C isothermal surface instead of 0°C leads to an increase of transport of more than a factor of five. The reason for these large differences is illustrated by Georgi's (1981) Figs. 11 and 12, which show that the vertical shear has the same sign and about the same magnitude over the temperature range between 0° and 2°C. The current-meter-based transport calculations of Whitworth et al. (1991) at 50°S are in turn very close to the modeled transport of 8.5 Sv, although these measurements also refer to water colder than 0.2°C. The only further measurements of WBC transports in the western basin are those of Whitehead and Worthington (1982) at 4°N yielding 0.8 Sv (model value 2.3 Sv) and Weatherly and Kelley (1982) at 40°N, which confirm at least the reversal of the WBC transport direction. A fundamental difference between the model results and observations exists in the western tropical Atlantic. Here the model diagnoses a northward WBC. Observations, however, indicate that there is no or only a weak WBC between about 8° and 16°N, and the entire northward LCDW transport occurs in the interior and on the eastern side of the basin (Fuglister 1960; Wright 1970; Whitehead and Worthington 1982).

The latitudinal change of transport in WBC No. 7 is not uniform but is interrupted by jumps where the transport changes rapidly. These jumps are either caused by abrupt changes of the width of the basin or by other WBCs separating from WBC No. 7 or flowing into it. The first determines the pathlength of the integral (2) and in turn leads to sudden modifications of the volume flux deficit in the western boundary layer. This is the case between 50° and 48°S where the WBC transport increases due to the widening of the Argentine Basin, at about 28°S because of the Rio Grande Rise, and north of 40°N caused by the narrowing of the Northwest Atlantic Basin. The latter occurs at 58°, 34°, and 2°S and 11°N due to WBCs Nos. 2, 6, 5, and 4.

The southern Cape–Agulhas Basin WBC (No. 2) separates from WBC No. 7 at 58°S and starts with a transport value of 2.6 Sv at the most southern extension of the Cape–Agulhas Basin. In the basin, the transport decreases with latitude and reaches a minimum value of 0.8 Sv at 52°S and then increases again to 2.7 Sv at 46°S. Farther north the transport decreases and suddenly drops from about 1.5 Sv to zero at 34°S. Right now, the northern Cape–Agulhas Basin WBC (No. 1) starts with northward transport of close to 1 Sv and gradually decreases to zero at 22°S. Hence, WBC No. 2 is absorbed by WBC No. 1 at the entrance of the Walvis Passage. Unfortunately, there exist no observations for comparison in this area.

WBC No. 4 branches from No. 7 at 11°N, which is the northern boundary of the Vema Fracture Zone. The initial transport is about 0.5 Sv northward. At 20°N the sign of the transport changes and to the north of this latitude only southward transport with a maximum of 1.4 Sv at 46°N can be found. This result is contrary to the geostrophic calculations of McCartney et al. (1991), who found a WBC beginning at the Vema Fracture Zone at 11°N and then flowing northward all along the eastern flank of the Mid-Atlantic Ridge up to about 30°N. They found a southward boundary current only at 36°N. In addition, the results disagree also quan-

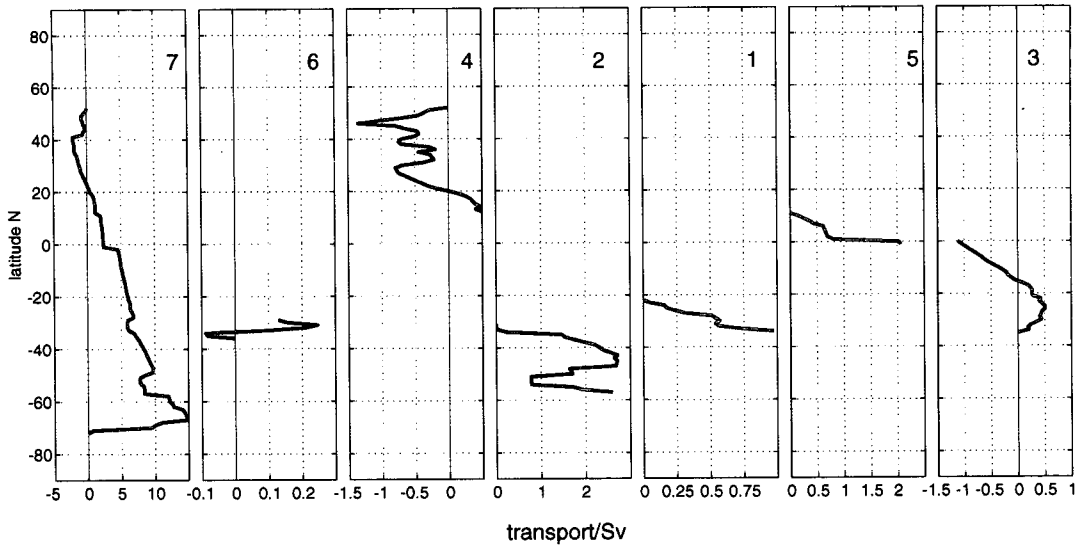

FIG. 5. Model run STDRD: transports in WBCs numbers 1 to 7 (cf. Fig. 2).

titatively. In the present study the northward WBC at the exit of the Vema Fracture Zone exhibits a maximum transport of 0.5 Sv, McCartney et al.'s (1991) WBC, however, is more than three times stronger.

The WBCs numbers 5 and 6 affiliated with "islands" are directed northward due to the choice of the starting point of the integration (see above) and are in agreement with observations, except for the most southern part of the Hunter Channel WBC that flows in the opposite direction. The only transport observations in the Hunter Channel (No. 6) have been published by Speer et al. (1992), who reported 0.7 Sv northward LCDW transport. Although the model value is only about 30% of that number, it does not make sense to discuss the difference because the model value depends strongly on the topographic shape, that is, on the channel width. In a few additional runs it has been found that converting one grid point on the eastern bank of the channel from "land" to "water" leads to an increase of the WBC transport by more than a factor of 2. The WBC at the eastern flank of the island in the tropical Atlantic is fed by a nearly 2 Sv northward flow through the Romanche Fracture Zone, more than one-half of which turns immediately to the east to supply the Angola Basin WBC (No. 3). The rest continues farther northward and the transport diminishes gradually to zero when approaching the Vema Fracture Zone at the northern end of the island. Starting the integration for this WBC at the southern end of the island yields a southward boundary current and an opposite flow through the Romanche Fracture Zone, which is in disagreement with observations (Metcalf et al. 1964; Heezen et al. 1964).

The Angola Basin WBC (No. 3) separates from the northward directed WBC No. 5 immediately after its beginning at the equator. The initial southward transport is about 1.1 Sv, but it diminishes rapidly to zero at 15°S. Between 15° and 34°S the WBC flows to the north, exhibiting maximum transport rates of 0.4 Sv. The sign of the transport is in agreement with the findings of Warren and Speer (1991), who calculated southward WBC flow at 11°S and northward flow at 24°S (cf. Table 1), but the magnitudes are partly different. In the southward regime the observations yield 0.75 Sv, which is close to the model value of 1.1 Sv; in the northward regime, however, the observed number of 2.45 Sv is nearly five times larger than the model value. The authors attribute this extraordinarily high transport to uncertainties in the geostrophic method and the superimposed noise of an Agulhas eddy.

b. *Interior flow and net meridional transports*

The interior flow outside the western boundary layer is displayed in Fig. 7a. According to (1) the meridional component is directed toward the pole on either hemisphere because w is positive everywhere except for the site of the concentrated source and $\tan\varphi$ has the same sign as the latitude. Together with the WBCs (Figs. 5, 6), this yields cyclonic flow patterns, where the WBCs are directed equatorward, that is, for the Argentine, Cape–Agulhas, and Brazil Basins, the southern part of the Angola Basin, and the northern parts of the Northwest and Northeast Atlantic Basins. Between the equator and 23°N, both the interior and WBC transports are directed poleward; hence, there is no closed circulation pattern. The same happens in the Angola Basin between the equator and 15°S.

A comparison with observations exhibits many similarities, but there are also regions where the modeled flow pattern deviates from the observed one. The cyclonic flow pattern in the Argentine Basin is confirmed

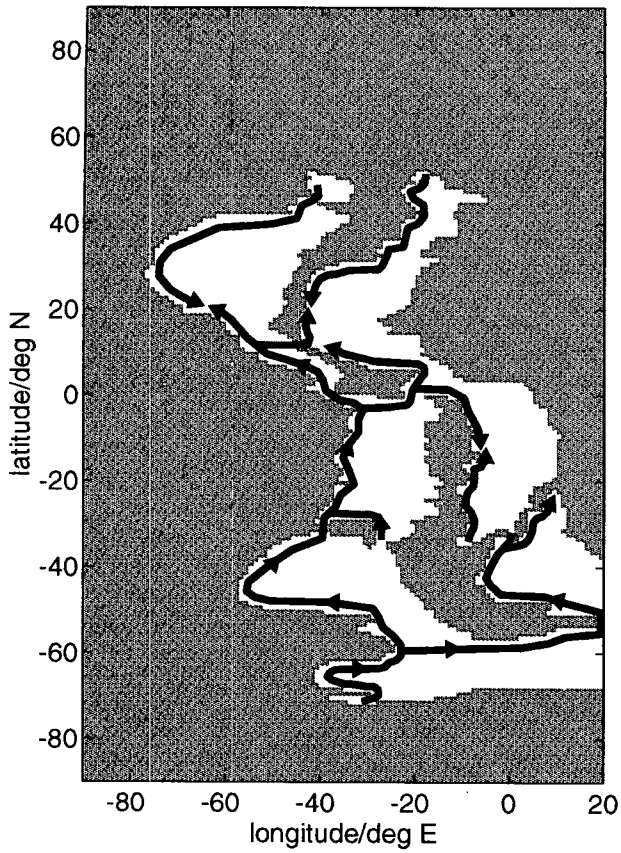

FIG. 6. Model run STDRD: a sketch displaying the pattern of western boundary currents.

by Reid's (1989) geostrophic flow analysis at the 4000 and 4500 dbar levels (his Figs. 29 and 30) and by the current-meter measurements of Whitworth et al. (1991). In contrast, Weatherly's (1993) investigations of near-bottom flow reveal some indication for an anticyclonic flow pattern. In the Cape–Agulhas Basin, both the model and Reid's (1989) calculations yield cyclonic flow (his Fig. 31). There is also good agreement in the Angola Basin, although there is no WBC visible in Reid's (1989) Fig. 30. The high-resolution survey of Warren and Speer (1991), however, matches the modeled pattern rather well. The situation is worse in the Brazil Basin, where none of the observations yields a cyclonic-flow pattern, but the observations also disagree among themselves. Reid's (1989) Figs. 29 and 30 suggest northward transport over the entire Basin, whereas in Wright's (1970) geostrophic calculations there is clear evidence for a concentrated northward western boundary flow at 32°, 24°, 16°, and 8°S and a regime with alternating flow directions in the eastern half of the Basin. A similar picture emerges also from the very recent publications of Speer and Zenk (1993) and Durrieu de Madron and Weatherly (1994), where the LCDW flow in the eastern Brazil Basin exhibits a complex structure of cyclonic and anticyclonic recirculation regimes.

The LCDW transport pattern in the Northeast Atlantic Basin has been investigated by McCartney et al. (1991). Although their transport rates for the interior flow are again about three times stronger than the modeled transports (like the WBCs, see above), a compar-

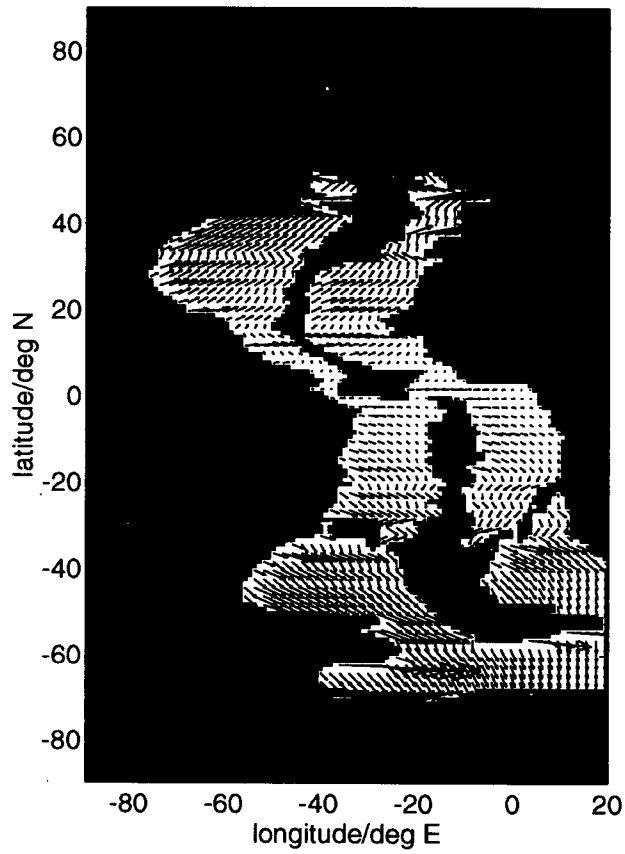

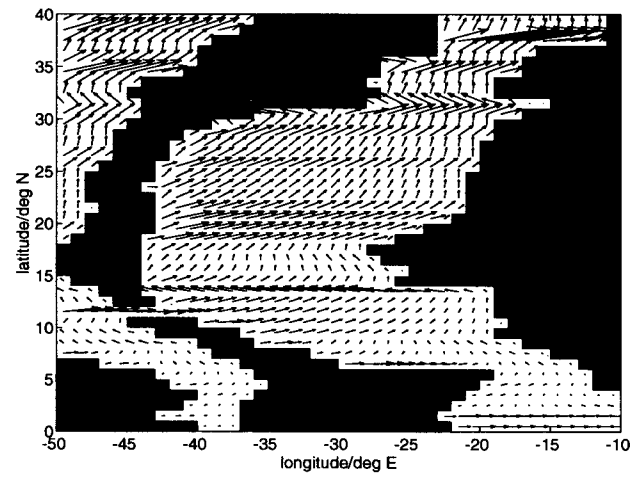

FIG. 7. Model run STDRD: interior volume transport (a) in the entire model domain and (b) in the tropical and subtropical northeast Atlantic. The length of the arrows is proportional to the transport.

ison of their summary sketch of observed transports (their Fig. 4) with the modeled pattern displayed in Fig. 7b reveals some striking qualitative similarities. Both in the observations and the model a jetlike current enters the Gambia Abyssal Plane (cf. their Fig. 1) through the Vema Fracture Zone. When approaching the African shelf, the jet becomes progressively weaker and turns cyclonically into a counterflow, the generation of which is obviously due to the blocking of northward transport by the Cape Verde Plateau. Farther to the north the flow direction changes again and northeasterly flow prevails throughout the basin. Please note that a WBC comparable to McCartney et al.'s (1991) northward WBC flow along the Mid-Atlantic Ridge is absent from Fig. 7b.

Except for some transport vectors in the Guiana (cf. Fig. 7b) and the Newfoundland Basins, the modeled interior flow in the Northwest Atlantic Basin is directed toward the northeast. It is difficult to compare the flow with findings from observations because these differ among themselves. Reid (1994, Fig. 81) suggests a northward bottom water flow at 4500 dbar along the Mid-Atlantic Ridge, which turns to the west at about 30°N and then to the east again at 35°–40°N. At the western boundary, southward flow is found all along the American coast. Schmitz and McCartney's (1993) circulation cartoons indicate northward flow all along the Mid-Atlantic Ridge and a system of several gyres to the west instead of a continuous western boundary flow. In contrast, the bottom temperature (McCartney et al. 1991, Fig. 2) and silica distribution (Mantyla and Reid 1983, Fig. 2e) indicate that the poleward LCDW transport occurs in two lobes branching at about 20°N. The western lobe is confined to the American shelf; the eastern lobe, however, extends over the central and eastern part of the basin and indicates a preferred flow direction toward the northeast as in Fig. 7a.

The net meridional LCDW volume transport across any latitude circle can be decomposed into the transport in the western boundary layer and the zonally integrated interior transport. Figure 8 displays the net and interior flow for the western (i.e., the Argentine, Brazil, and Northwest Atlantic Basin) and the eastern basin (the Angola, Cape–Agulhas, and Northeast Atlantic Basin). The differences between both curves are the WBC transports. In the western basin (Fig. 8a) the net transport is to the north everywhere, decreasing monotonically from 6.6 Sv at 54°S to zero at the northern limit of the basin. The interior transport, however, changes sign at the equator. Therefore, the entire cross equatorial transport of nearly 2.6 Sv occurs in the WBC. At 23°N the curves for the interior and the net transports are crossing, which means that the WBC is changing sign and the northward transport occurs solely in the interior. Thus, we can distinguish between three regimes—a "western boundary current regime" on the Southern Hemisphere where the sign of the WBC determines the sign of the net flow, a "mixed

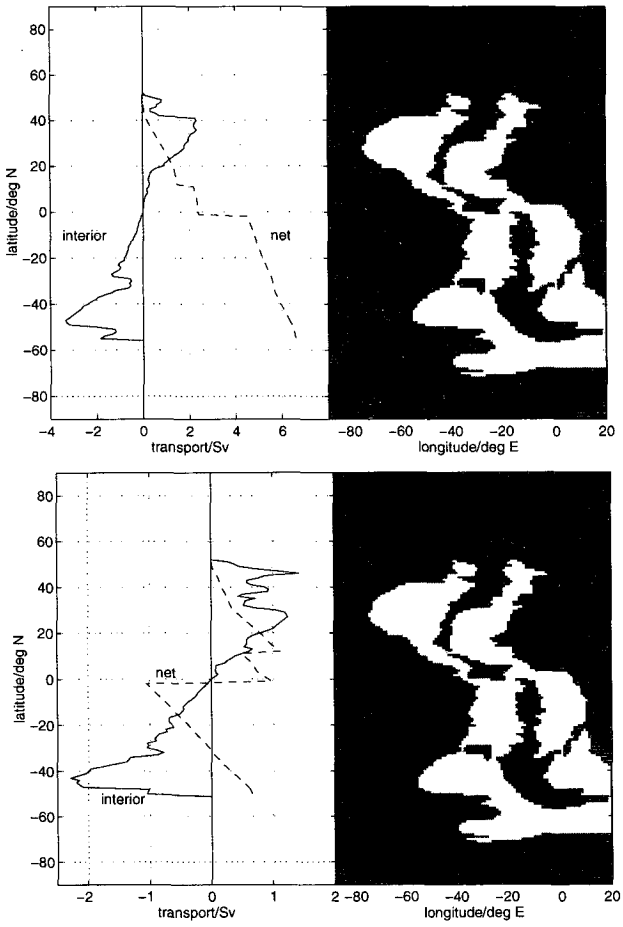

FIG. 8. Model run STDRD: net and interior transports (a) in the western and (b) in the eastern basin. The highlighted areas (right panel) indicate the respective basin.

regime" between the equator and 23°N where the WBC and the interior flow both contribute to the northward net transport, and an "interior regime" to the north of that latitude where the net transport is governed by the sign of the interior flow. Available consistent observations are the WBC and net transport measurements at 4°N [McCartney (1994); Whitehead and Worthington (1982), cf. Table 1], indicating that both the interior and the WBC flow are positive, and the measurements of Georgi (1981) at 56° and 59°S in the Weddell–Enderby Basin suggesting an interior flow opposed to the WBC. In addition, it should be mentioned that the observed net transports of the entire western basin are consonant with the modeled transport rates by definition (cf. section 3).

In the eastern basin (Fig. 8b) the situation is somewhat more complicated. As in the western basin, the interior flow is poleward in both hemispheres; the net flow, however, is southward in the Angola Basin and northward in the Cape–Agulhas Basin and north of 2°S. The crossing of both curves occurs at the locations

of the WBC sign changes at 15°S in the Angola Basin, at 2°S, where the Angola Basin WBC branches from the northward continuing WBC No. 5 and at 20°N in the Northeast Atlantic Basin. Hence, using the same definitions as in the western basin, the eastern basin is fundamentally different from the western basin; it is a "western boundary regime" in the Cape–Agulhas Basin and an "interior regime" north of 20°N and in the Angola Basin south of 15°S because both the interior transport and the net transport exhibit the same sign and are opposed by the WBC. Except for the small latitude band between 2°S and the equator, the rest of the eastern basin is a "mixed regime."

Combining both the net flow in the western and eastern basin allows comparison with Roemmich and Wunsch's (1985) inverse calculation between 24 and 36°N. They find a net northward bottom water flow of 2.9 ± 2.6 Sv, which is comparable to the modeled net flow of about 1.5 Sv in the same latitude range.

5. Discussion

The above comparison of model results with observations has shown that there is at least a qualitative agreement in most parts of the Atlantic. In some locations a comparison is impossible because lack of observations, but there are also regions where the model results and the observations disagree. These differences can either be explained by necessarily somewhat arbitrary assumptions in the interpretation of hydrographic data or they are due to shortcomings of the model formulation.

A first significant difference occurs in the Northeast Atlantic Basin. In contrast to McCartney et al. (1991), who found only northward WBC transports, the model yields a sign change of the WBC confined to the eastern flank of the Mid-Atlantic Ridge at about 20°N. As the other modeled reversals of WBC direction in the Angola Basin and in the Northwest Atlantic Basin are confirmed by the few available observations, it is assumed that McCartney et al.'s (1991) different findings are possibly caused by their fairly warm reference level between 2° and 2.5°C, which makes the LCDW transport stronger in regions where the overlying Deep Water moves in the opposite direction and may reverse the sign of the LCDW flow, where both water masses move in the same direction. The latter has possibly caused the observed northward WBC flow north of 20°. Another fact pointing to the possibility that the reference level is too warm is that the observed interior transports agree qualitatively with the model but are stronger by at least a factor of 3. In addition, the Vema Fracture Zone throughflow of 2.2 Sv is more than two times the modeled value of about 0.9 Sv (interior plus WBC transport) and nearly five times the transport observed by Vangriesheim (1980). In a series of extra model model runs, it was found that a transport of 2 Sv through Vema Fracture Zone could only be achieved by doubling the LCDW production rate, which in turn yields extremely unrealistic results for other regions.

Another disagreement worth mentioning is the interior flow in the Brazil Basin, the observed structure of which is obviously more complex than in the model. A possible explanation for the observed alternating directions of the meridional flow has recently been offered by Spall (1994). He applied a three-dimensional primitive equations model to an idealized basin, which is comparable in size to the Brazil Basin, and found that instabilities of the western boundary current alter the mean basin-scale deep flow from a cyclonic to an anticyclonic recirculation.

Observations suggest that the northward LCDW flow flips from the western to the eastern side of the Guiana Basin after crossing the equator; that is, in the western tropical Atlantic a WBC as predicted from the model is absent. Speer and McCartney (1992) demonstrated that this can be due to a variable thickness of the LCDW layer, and Warren (1981) and Pedlosky and Chapman (1993) proposed the meridional topography slope to generate this flow pattern. Another possibility is that the LCDW transport pattern is affected by the complicated topography or it is steered by the overlying strong cyclonic recirculation cell of North Atlantic Deep Water (cf. Friedrichs et al. 1994). Nof and Olson (1993) using a $1\frac{1}{2}$ and a $2\frac{1}{2}$ layer analytical model could show that the flipping is simply a consequence of geostrophy applied to a deep boundary current jet, which is separated by a front from the interior of the ocean. All these effects could not be investigated in the present study because of the flat bottom and the uniform layer thickness and will be subject of a later paper.

Georgi's (1981) transport calculations in the South Sandwich Trench at 56° and 59°S (cf. Table 1) yielded extraordinarily high transport values of up to 15 Sv net meridional flow and transport rates of 18 Sv in the WBC. In the model, comparable values could only be archieved assuming a LCDW formation rate of at least 12 Sv, but this generates WBC and net meridional transports in the western basin incompatible with observations (Fig. 4). However, if the excess LCDW is allowed to flow into the Indian Ocean, higher formation rates are possible without affecting the transport rates in the Atlantic Basins. In an additional model run (INDIAN), the formation rate was increased to 13 Sv and the surplus of 5 Sv was absorbed by a sink smeered out over the latitude range between 60° and 56°S along the eastern boundary, where the LCDW outflow seems to occur according to Reid (1989, his Fig. 30). The resulting WBC structure (Fig. 9) north of 56°S is the same as in the previous model run, but south of that latitude the transport has increased to nearly 20 Sv at 66°S. Hence, it is in principal possible to say Georgi's (1981) large transports are caused by a significant LCDW outflow into the Indian Ocean, the magnitude of which, however, is not known from measurements. It should be noted that from Georgi's (1981) measure-

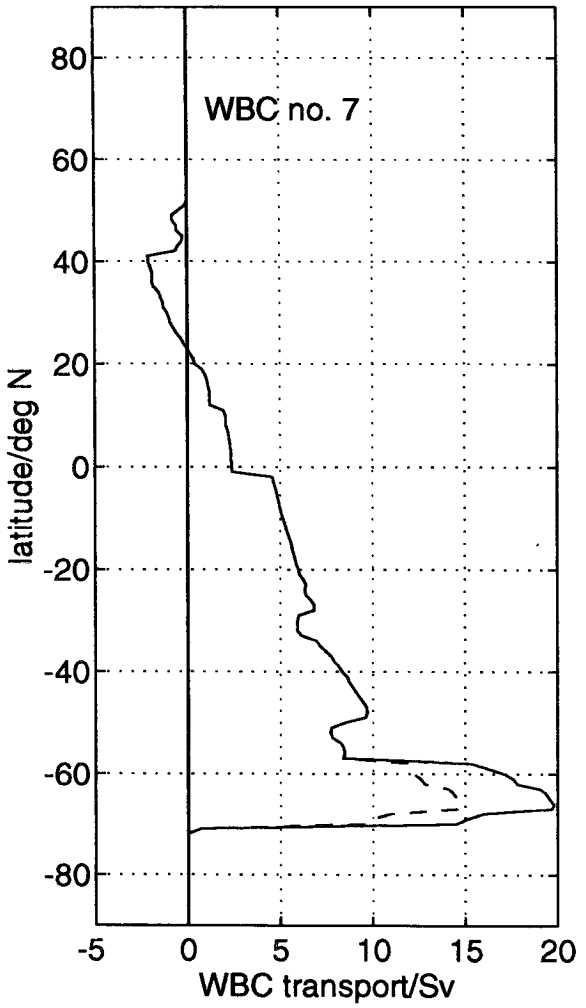

FIG. 9. Model run INDIAN: transport rates in the western Atlantic WBC driven by an enhanced LCDW formation rate of 13 Sv (solid line). The dashed line shows for comparison the transport of model run STDRD using a formation rate of 8 Sv. The excess LCDW of 5 Sv escapes to the Indian Ocean.

ments even higher transport values are possible if a warmer reference level would have been chosen (cf. the sign of the vertical shear in his Figs. 6–8).

The probable most crucial assumption in the model is the uniform upwelling of LCDW over the entire Atlantic. According to (1) and (2), w determines the structure of the interior flow, the divergence of which affects the strength of the WBC. In order to find out to what degree a nonuniform upwelling affects the model results, four further model runs driven by different upwelling patterns have been accomplished. In each of these runs the upwelling was increased by 50% in a selected area in comparison with the uniform upwelling case. The upward flux over the rest of the model domain was then reduced to a value closing the volume flux budget. In model run NORTH, the upwelling was increased in the North Atlantic, and in SOUTH, WEST, and EAST accordingly in the south, west, and east Atlantic. If in each of these runs the LCDW formation rate was kept at 8 Sv, this would lead to net meridional transport rates in the western basin very different from the observed values. Therefore, the LCDW formation rate in every run was adjusted to match approximately the transport value of STDRD at 30°S, which was 5.64 Sv. This latitude was chosen because it is probably one of the best observed sites of net LCDW flow in the Atlantic. The formation rate, the vertical speed $\bar{w}$ for the uniform upwelling case, and the enhanced (highlighted in Fig. 10) and reduced vertical speeds (gray shaded), w_H and w_L, respectively, are summarized for these four runs in Table 2 together with the respective values of STDRD. In order to visualize the effect of different upwelling patterns, the western basin net transports are displayed in Fig. 10. The surprising result is that in NORTH, EAST, and WEST the transports are very close to those in STDRD (dotted); the maximum difference of about 0.8 Sv occurs in NORTH between the equator and about 10°N. Larger differences of up to 1.4 Sv can be found in SOUTH in the same latitude range. Comparing all four graphs among each other reveals that the cross equatorial flow and the flow through the Romanche Fracture Zone are the quantities that respond most sensitively to modifications of the upwelling pattern. In SOUTH the cross equatorial flow is only about 1 Sv, whereas in NORTH it is more than 3 Sv. The Romanche Fracture Zone throughflow (i.e., the width of the step in the graphs at about 2°S), however, exhibits a minimum value of 1.3 Sv in WEST and a maximum between 2.5 and 3 Sv in SOUTH and EAST. A comparison with the observations reveals that in NORTH and WEST nearly all transports on the Northern Hemisphere are too large, whereas in SOUTH the Northern Hemisphere transports are too low. On the other hand, the Southern Hemisphere transports in EAST seem to be too strong. Hence, it is rather speculative as to which upwelling pattern matches best the observed transports, it is probably a combination of several ones. However, the above results have shown that the STDRD transport pattern is rather robust with respect to different assumptions regarding the large-scale distribution of upwelling.

6. Conclusions

The above model study has shown that applying the linearized vorticity equation to a uniform thickness layer yields reasonable results for the spreading of Lower Circumpolar Deep Water (LCDW) in the Atlantic Ocean. In contrast to Stommel (1958), who calculated the deep circulation as an integral over the deep and bottom water masses assuming two sources in the northern North Atlantic and in the Weddell Sea, only the LCDW containing layer is considered here. The formation of Atlantic LCDW is simulated by a single source located in the Weddell Sea representing the gain

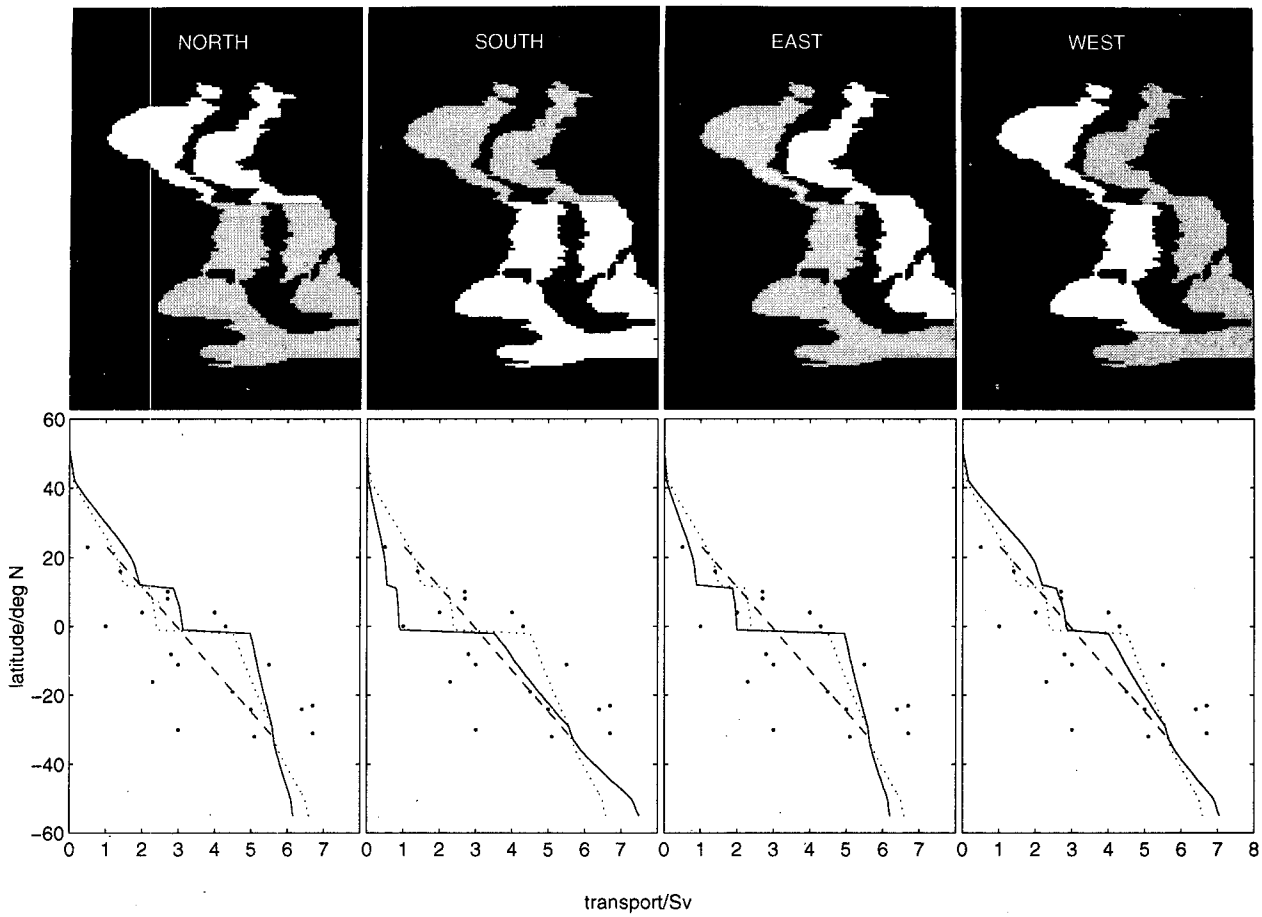

FIG. 10. Upper panel: in model runs NORTH, SOUTH, EAST, and WEST the upwelling was increased by 50% in the highlighted areas in comparison to the uniform upwelling case. In the gray shaded areas the upwelling was reduced accordingly to balance the LCDW production rate. Lower panel: the corresponding net meridional transports in the western basin. The dotted curve is the net transport for the STDRD run, and the dashed line represents the linear regression fitted to the observed net transports (dots, cf. Figs. 3, 4).

from the Circumpolar Current and production in the Weddell Sea. Another feature of this study is that the net meridional flow in the western Atlantic Basin is calibrated against a linear fit of observed transport rates. This allows one to put a lower bound on the LCDW gain of the Atlantic Ocean, the value of which lies between 6.9 an 10.1 Sv depending on the selected upwelling pattern compensating for the LCDW production. The gross production of LCDW in the Atlantic sector of the Southern Ocean, that is, the inflow through Drake Passage plus the total production in the Weddell Sea, must be higher, however, because an unknown fraction is lost to the Indian Ocean.

Regardless of the choice of the upwelling distribution, the net meridional Atlantic LCDW transport pattern consists of interior transports and a system of west-

TABLE 2. Comparison of forcing parameters in model runs STDRD, NORTH, SOUTH, EAST, and WEST. The symbols have the following meaning: $\bar{w}$ upwelling speed for the uniform upwelling case, w_H enhanced upwelling speed in highlighted areas in Fig. 10, w_L reduced vertical speed in gray shaded areas in Fig. 10.

Run	Production rate (Sv)	$\bar{w}$ (10^{-7} m s^{-1})	w_H (10^{-7} m s^{-1})	w_L (10^{-7} m s^{-1})
STDRD	8.0	1.7	—	—
NORTH	6.9	1.5	2.3	1.0
SOUTH	10.2	2.2	3.3	0.6
EAST	7.6	1.7	2.5	1.0
WEST	7.8	1.7	2.6	0.9

ern boundary currents. As their relative contributions to the net transport vary from place to place, the model offers a primitive tool to calculate either of these quantities if the other is known from observations. In addition, the model results provide estimate values to test the consistency of transport measurements at different locations.

Acknowledgments. This work is a contribution to Grant 03F0121A of the German Bundesministerium für Forschung und Technologie.

REFERENCES

Amos, F., A. L. Gordon, and E. D. Schneider, 1971: Water masses and circulation patterns in the region of the Blake–Bahama Outer Ridge. *Deep-Sea Res.*, **18,** 145–165.

Carmack, E. C., 1977: Water characteristics of the Southern Ocean south of the Polar Front. *A Voyage of Discovery,* M. Angel, Ed., Pergamon, 15–41.

——, and T. D. Foster, 1975: On the flow of water out of the Weddell Sea. *Deep-Sea Res.*, **22,** 711–724.

Connary, S. D., and M. Ewing, 1974: Penetration of Antarctic Bottom Water from the Cape Basin into the Angola Basin. *J. Geophys. Res.*, **79**(C3), 463–469.

Durrieu de Madron, X., and G. Weatherly, 1994: Circulation, transport and bottom boundary layers of the deep currents in the Brazil Basin. *J. Mar. Res.*, **52,** 583–638.

Eittreim, S. L., P. E. Biscaye, and S. S. Jacobs, 1983: Bottom water observations in the Vema fracture zone. *J. Geophys. Res.*, **88**(C4), 2609–2616.

Emery, W. J., and J. Meincke, 1986: Global water masses: Summary and review. *Oceanol. Acta,* **9,** 383–391.

Foster, T. D., and E. C. Carmack, 1976: Frontal zone mixing and Antarctic Bottom Water formation in the southern Weddell Sea. *Deep-Sea Res.*, **23,** 301–317.

Friedrichs, M. A. M., M. S. McCartney, and M. M. Hall, 1994: Hemispheric asymmetry of deep water transport modes in the Atlantic. *J. Geophys. Res.*, **99**(C12), 25 165–25 179.

Fuglister, F. C., 1960: *Atlantic Ocean Atlas of Temperature and Salinity Profiles and Data from the International Geophysical Year of 1957–1958.* Vol. I, Woods Hole Oceanographic Institution Atlas Series, 209 pp.

Georgi, D. T., 1981: Circulation of bottom waters in the southwestern South Atlantic. *Deep-Sea Res.*, **28A,** 959–979.

Gill, A. E., 1973: Circulation and bottom water production in the Weddell Sea. *Deep-Sea Res.*, **20,** 111–140.

Gordon, A. L., 1966: Potential temperature, oxygen and circulation of bottom water in the Southern Ocean. *Deep-Sea Res.*, **13,** 1125–1138.

Heezen, B. C., E. T. Bunce, J. B. Hersey, and M. Tharp, 1964: Chain and Romanche Fractur zones. *Deep-Sea Res.*, **11,** 11–33.

Hogg, N. G., P. Biscaye, W. Gardner, and W. J. Schmitz Jr., 1982: On the transport and modification of Antarctic Bottom Water in the Vema Channel. *J. Mar. Res.*, **40**(Suppl.), 231–263.

Mantyla, A. W., and J. L. Reid, 1983: Abyssal characteristics of the World Ocean waters. *Deep-Sea Res.*, **30A,** 805–833.

McCartney, M. S., 1994: The transport of Antarctic Bottom Water at 4°N in the western basin of the North Atlantic Ocean. *J. Phys. Oceanogr.,* in press.

——, and R. A. Curry, 1993: Transequatorial flow of Antarctic bottom water in the western Atlantic Ocean: Abyssal geostrophy at the equator. *J. Phys. Oceanogr.*, **23,** 1264–1276.

——, S. L. Bennett, and M. E. Woodgate-Jones, 1991: Eastward flow through the Mid-Atlantic Ridge at 11°N and its influence on the abyss of the eastern basin. *J. Phys. Oceanogr.*, **21,** 1089–1121.

Metcalf, W. G., B. C. Heezen, and M. C. Stalcup, 1964: The sill depth of the Mid-Atlantic Ridge in the equatorial region. *Deep-Sea Res.*, **11,** 1–10.

Nof, D., and D. B. Olson, 1993: How do western abyssal currents cross the equator? *Deep-Sea Res.*, **40** I, 235–255.

Pedlosky, J., and D. C. Chapman, 1993: Baroclinic structure of the abyssal circulation and the role of meridional topography. *J. Phys. Oceanogr.*, **23,** 979–991.

Reid, J. L., 1989: On the total geostrophic circulation of the South Atlantic Ocean: Flow patterns, tracers and transports. *Progress in Oceanography,* Vol. 23, Pergamon, 149–244.

——, 1994: On the total geostrophic circulation of the North Atlantic Ocean: Flow patterns, tracers and transports. *Progress in Oceanography,* Vol. 33, Pergamon, 1–92.

——, W. D. Nowlin, and W. C. Patzert, 1977: On the characteristics and circulation in the southwestern Atlantic Ocean. *J. Phys. Oceanogr.*, **7,** 62–91.

Rintoul, S. R., 1991: South Atlantic interbasin exchange. *J. Geophys. Res.*, **96**(C2), 2675–2692.

Roemmich, D., and C. Wunsch, 1985: Two transatlantic sections: Meridional circulation and heat flux in the subtropical North Atlantic Ocean. *Deep-Sea Res.*, **32,** 619–664.

Saunders, P. M., 1987: Flow through Discovery Gap. *J. Phys. Oceanogr.*, **17,** 631–643.

Schmitz, W. J., Jr., and M. S. McCartney, 1993: On the North Atlantic circulation. *Rev. Geophys.*, **31,** 29–49.

Spall, M. A., 1994: Wave induced abyssal recirculations. *J. Mar. Res.*, **52,** 1051–1080.

Speer, K. G., and M. S. McCartney, 1992: Bottom water circulation in the western North Atlantic. *J. Phys. Oceanogr.*, **22,** 83–92.

——, and W. Zenk, 1993: The flow of Antarctic Bottom Water into the Brazil Basin. *J. Phys. Oceanogr.*, **23,** 2667–2682.

——, ——, G. Siedler, J. Pätzold, and C. Heidland, 1992: First resolution of bottom water flow through the Hunter Channel in the South Atlantic. *Earth Planet. Sci. Lett.*, **113,** 287–292.

Stommel, H., 1958: The abyssal circulation. *Deep-Sea Res.*, **5,** 80–82.

Sverdrup, H. U., M. W. Johnson, and R. H. Fleming, 1942: *The Oceans.* Prentice Hall, 1087 pp.

Tucholke, B. E., W. R. Wright, and C. D. Hollister, 1973: Abyssal circulation over the Great Antilles Outer Ridge. *Deep-Sea Res.*, **20,** 973–995.

Vangriesheim, A., 1980: Antarctic Bottom Water flow through the Vema fracture zone. *Oceanol. Acta,* **3,** 199–207.

Warren, B. A., 1981: Deep circulation of the World Ocean. *Evolution of Physical Oceanography,* Warren and Wunsch, Eds., MIT Press, 6–41.

——, and K. G. Speer, 1991: Deep circulation in the eastern South Atlantic. *Deep-Sea Res.*, **38**(Suppl. 1), S281–S322.

Weatherly, G. L., 1993: On deep current and hydrographic observations from a mudwave region and elsewhere in the Argentine Basin. *Deep-Sea Res.*, **40** II(4,5), 939–961.

——, and E. A. Kelley Jr., 1982: 'Too cold' bottom layers at the base of the Scotian Rise. *J. Mar. Res.*, **40,** 985–1012.

——, and ——, 1985: Two views of a cold filament. *J. Phys. Oceanogr.*, **15,** 68–81.

Whitehead, J. A., Jr., and L. V. Worthington, 1982: The flux and mixing rates of Antarctic Bottom Water within the North Atlantic. *J. Geophys. Res.*, **87**(C10), 7903–7924.

Whitworth, T., III, W. D. Nowlin, R. D. Pillsbury, M. I. Moore, and R. F. Weiss, 1991: Observations of the Antarctic Circumpolar Current and deep boundary current in the Southwest Atlantic. *J. Geophys. Res.*, **96**(C8), 15 105–15 118.

Wright, W. R., 1970: Northward transport of Antarctic Bottom Water in the western Atlantic Ocean. *Deep-Sea Res.*, **16**(Suppl.), 433–446.